12-15-2014

Temporal Constraints on Holocene Initiation and Termination of Mound Development at an Episodic Gas Hydrate and Cold Seep System, Woolsey Mound, Northern Gulf of Mexico

Nathan Robinson
University of South Carolina - Columbia

TEMPORAL CONSTRAINTS ON HOLOCENE INITIATION AND TERMINATION OF MOUND DEVELOPMENT AT AN EPISODIC GAS HYDRATE AND COLD SEEP SYSTEM, WOOLSEY MOUND, NORTHERN GULF OF MEXICO

by

Nathan Robinson

Bachelor of Science
University of South Carolina, 2013

Submitted in Partial Fulfillment of the Requirements

For the Degree of Master of Science in

Geological Sciences

College of Arts and Sciences

University of South Carolina

2014

Accepted by:

James H. Knapp, Director of Thesis

Howie Scher, Reader

Robert Thunell, Reader

Lacy Ford, Vice Provost and Dean of Graduate Studies

ACKNOWLEDGEMENTS

First I would like to thank my family and friends who provided support throughout my educational experience, especially my mother Mary Louise Robinson and my father Heyward Robinson. Special thanks to my undergraduate and graduate advisor, Dr. James Knapp, who provided support and guidance throughout my collegiate career. I would like to thank the Bureau of Ocean Energy Management and the Gulf of Mexico Hydrate Research Consortium for providing data used in this project. I thank Dr. Charlotte Brunner with The University of Southern Mississippi for providing access to sediment cores and her assistant Franklin Williams in the sampling process. I thank Dr. Wesley Ingram and Dr. Stephen Meyers for allowing the use of their oxygen isotope data. I thank the Marine Sediments Research Lab at the University of South Carolina for guidance through picking foraminifera, materials, facilities, and mass spectrometer usage. Special thanks to my committee members Dr. Howie Scher and Dr. Robert Thunell for advice and insight throughout the project. Finally, I would like to thank the students from the Tectonics and Geophysics Lab and the Geophysical Exploration Lab for fellowship and support.

ABSTRACT

Woolsey Mound is a thermogenic gas hydrate and cold seep system in the deepwater (900m) Gulf of Mexico. A set of sub-bottom seismic profiles acquired at MC-118 Woolsey Mound provide decimeter-scale vertical resolution of the upper ~50m of the subsurface throughout the lease block. Integration of these data with radiocarbon, lithostratigraphic, and biostratigraphic data from shallow gravity cores provides the basis for detailed interpretation of the mound evolution within the last 12,000 years. Uniform sedimentation during the Last Glacial Maximum and following changes in sediment distribution over MC-118 suggests modern mound activity did not begin until at least ~12ka. Development of the mound system appears to be related to salt tectonism, and was characterized in sequence by (1) formation of NNE-trending folds (~10 m structural relief), (2) shallow normal faulting (1-2 m apparent offsets), (3) subsea erosion of the mound superstructure, and (4) deposition of a sedimentary drape across the entire modern mound edifice. The base of the sedimentary drape sits in angular unconformity with the underlying folded, faulted, and eroded strata, and is dated to be no younger than 4 ka, suggesting the modern mound developed within a period of <8ka, and had assumed its current configuration by 4 ka. If correct, the mound, and by analogy, the cold seep and hydrate system, was entirely inactive until after the Last Glacial Maximum. These data place the first quantitative temporal constraints on the development of an episodic hydrate mound and associated cold seep system.

TABLE OF CONTENTS

LIST OF FIGURES

List of Abbreviations

LGM..... Last Glacial Maximum

MC-118.....Mississippi Canyon Lease Block 118

JPC.....Jumbo Piston Cores

INTRODUCTION

Deep-water cold seeps are geologic feature expressed by gas leaking through the hydrate stability zone and to the seafloor. This process is observed in marine environments worldwide (Judd and Hovland, 2007 and reference therein). These sites are the interest of multiple disciplines because they may affect climate change by the release of the potent greenhouse gas methane (Solomon et al., 2009, Dickens et al., 1995), and ocean acidification by the release of hydrocarbons into the water column (Biastoch et al., 2011). Furthermore, chemosynthetic life is dependent on the leaking gas, economical concentrates of gas hydrates may be present where there are free gas conduits through the hydrate stability zone (Nouze et al., 2004), and slope stability may be effected by gas hydrate dissociation (Hornbach et al., 2007).

CHAPTER 1

TEMPORAL CONSTRAINTS ON HOLOCENE INITIATION AND TERMINATION OF MOUND DEVELOPMENT AT AN EPISODIC GAS HYDRATE AND COLD SEEP SYSTEM, WOOLSEY MOUND, NORTHERN GULF OF MEXICO

1.1 INTRODUCTION

Currently, cold seeps are temporally poorly understood on a long-term (hundreds to millions of years) time scale (Bangs et al. 2013), but are better understood on a short-term time scale (Bangs et al. 2013; Kannberg et al. 2013; Boles et al. 2001; Macelloni et al., 2013). On a short-term time scale, cold seep flux of hydrocarbons are affected by hydrate formation/dissociation, temperature and pressure variations exerted on the systems, and temperature, salinity, and pressure variations within the system. Addressing the long-term mechanisms controlling cold seeps, and the time-frame in which cold seeps operate may provide insight into how these geologic features affect climate change, chemosynthetic life, and ocean acidifications.

Favorable conditions for methane seepage have been proposed during sea-level lowstands due to relatively low hydrostatic pressure on gas hydrates and seep systems (Tong et al., 2013; Watanabe et al., 2008; Kiel et al., 2009; Teichert et al., 2003; Wirsig et al., 2012). Other favorable conditions may include changes in bottom-water temperatures that affect gas hydrates (Kiel, 2009) salt diapirism (Roberts and Aharon, 1994; Aharon et al., 1997; Feng et al., 2010; Roberts and Carney, 1997; Bian et al., 2013; Roberts et al., 1990) and other structural/sediment deformation (Bangs et al., 2010;

Bayon et al., 2009a, Bayon et al., 2009b; Mazumdar et al., 2009). Methane derived authigenic carbonates are often used as chronometers for methane seepage (Kutterolf et al., 2008; Tong et al., 2013, Aharon et al., 1997 and references therein). Previous studies have dated seepage by U/Th dating of these authigenic carbonates and have found seepage activation to have occurred both within sea-level high and sea-level lows (Aharon et al., 1997; Bayon et al., 2009; Kutterolf, 2008; Teichert et al., 2003; Mazumdar et al., 2009; Feng et al., 2010; Liebetrau et al., 2010; Tong et al., 2013, Wirsig et al., 2012). This study provides a unique approach of temporal constraints based off integration of published sediment core data, radiocarbon, biostratigraphic, and δ 18O isotopic data with high-resolution seismic data. An interdisciplinary approach of stable isotope chemistry, sedimentology, and seismic analysis provides a dynamic understanding of this system. This method provides an understanding of time-variant mechanism affecting mound activity and geological forcing of seep activity. Understanding the relationship between cold seep activity and sea level will provide insight into the past and future of cold seeps and their relationship to tectonics.

1.2 REGIONAL SETTING

The Gulf of Mexico is a prolific hydrocarbon basin dominated by salt movement which complicate subsurface structures and seafloor bathymetry. There are over 21,000 cold seep sites (Shedd, 2012), and ~22,000 TCF of gas hydrates in the Gulf of Mexico (Bosewell et al., 2012). Woolsey Mound is a cold seep site located on the continental slope ~170 km south of Pascagoula, Mississippi and ~50 km from the Mississippi River delta in the lease block Mississippi Canyon-118 (MC-118) (Figure 1). It is located on the salt-dominated continental slope in ~900m water depth. MC-118 lease block has been

assigned by the Bureau of Ocean Energy Management as the long-term research reserve for the Gulf of Mexico Hydrates Research Consortium and has a seafloor observatory with a variety of apparatuses that measure biological, geochemical and geophysical data associated with Woolsey Mound (Simonetti et al., 2013; Lutkne et al., 2006 and 2011; Sassen et al., 2006; Ingram et al., 2010, 2013). The ~1km^2 field exhibits features diagnostic of a cold seep where hydrocarbon rich fluid migrate to the seafloor and create authigenic carbonates, chemosynthetic communities, gas hydrates, natural gas vents, and reefs (Woolsey et. al., 2005; Sassen et al., 2006; Macelloni et al, 2013, 2012; Sleeper et al., 2006). Salt tectonics have generated an intricate network of faults (Figure 2), creating hydrocarbon migration pathways for thermogenic gas from deep petroleum reservoirs up to the seafloor (Macelloni et al., 2012; Sassen et al., 2006). Transient hydrocarbon migration processes along the faults may lead to temporary instability for gas hydrates, making Woolsey Mound a very dynamic setting. Gas hydrate/carbonate mounds formed by cold seeps contain many structural and stratigraphic components that may be used to evaluate time-variant mechanisms affecting cold seep related activity. Current short-term hydrocarbon flux at Woolsey Mound is influenced by hydrates that have been collected through cores along the faults and imaged with seismic (Macelloni et al., 2012, Simonetti et al., 2013). This study attempts to address the long-term flux of hydrocarbons at Woolsey Mound and will be compared with other cold-seep sites in the Gulf of Mexico.

1.3 MATERIALS AND METHODS

1.3.1 SEISMIC DATA

In 2005 C&C Technology Autonomous Underwater Vehicle Hugin 3000 collected 25 E-W and 2 N-S lines CHIRP reflection lines over the MC-118 lease block with an E-W line

spacing of 200 meters. This CHIRP seismic data has a vertical resolution of ~0.1 m, providing a very high resolution image of the subsurface**.** Acquisition parameters include a frequency modulated between 2 and 8 kHz, a record length of 300 ms, and a 63-ms sampling interval. Details about CHIRP collection can be found at Sleeper et al. (2006). CHIRP seismic data was outputted in SEG-Y format and imported into Kingdom Suite SMT for further analysis. A time-depth conversion was applied to the seismic data using an average velocity of 1500 m/s in order to tie sediment cores with seismic data. There is an uncertainty in the degree of precision, but this does not significantly change structural and stratigraphic relationships. Depth converted seismic data was integrated with the sediment cores and was used to relate seismic signatures with different lithologies and ages, providing chronostratigraphic boundaries. This provides a mechanism to understand sedimentation throughout the area in time. Temporal constraints on structural and stratigraphic features of the mound system are inferred by dated horizons provided by published sediment cores (Ingram et al. 2010, Ingram et al. 2013) and sediment core analysis done through this project. Isochore maps are made by subtracting mapped horizons depths from each other, revealing sediment thickness throughout the study area. Comparing sediment thickness with the associated times of the horizons reveals variations in deposition rates. Understanding these components can further constrain mound activity and associated sedimentation surrounding the mound. Focus was given on the shallow sediment and structure which appears to reveal operations of the most recent phase of Woolsey Mound. Further seismic analysis of data collected over Woolsey Mound can be found in Macelloni et al., (2012). Previous phases of mound activity in the area is documented with deeper seismic data (Simonetti, Antonello, 2013).

1.3.2 “RED BAND” AND CHRONOSTRATIGRAPHY

Ingram et al. (2010, 2013) provides lithostratigraphy, biostratigraphy, and chronostratigraphy for MC-118 shallow sediment cores. These studies provided insight into sedimentation and stratigraphy surrounding Woolsey Mound (Ingram et al. 2010, 2013). Particular focus was given to a red band, identified by a negative $\delta^{18}O$ excursion and visibly red oxidized terrigenous sediment (Ingram et al. 2010, Ingram et al. 2013). This band has been linked to the deglaciation and meltwater pulse 1A (Ingram et al. 2010, Ingram et al. 2013). Biostratigraphic and radiocarbon dates constrain deposition of this ~1-2cm thick unit to ~14.5ky (Ingram et al. 2010). Meltwater pulse 1A was a period of rapid sea-level rise during the latest sea-level transgression and occurred within ~14.5-13 ky ago (Richard Fairbanks, 1989). The red band is marked by a distinct horizon in the seismic data and was mapped throughout the study area as a key horizon.

1.3.3 AUTHIGENIC CARBONATES

Methane derived authigenic carbonates precipitate in deep water cold seep settings and are used as an indicator of methane seepage. Anaerobic oxidation of methane causes favorable conditions for authigenic carbonate precipitation (Bayon et al., 2009). Authigenic carbonates are distinguishable from surrounding sediments because their high acoustic impedance compared to unconsolidated slope sediments (Taylor et al., 2010). Radiometric dating of authigenic carbonates has been used as a proxy for dating methane seepage, but this type of study has not been done in our study area.

1.3.4 JUMBO PISTON CORES

Jumbo Piston Cores (JPC) were collected over the mound in January, 2011 to acquire deep (up to 20 m b.s.f) geological, geochemical and geophysical data (Simonetti

et al., 2013). Specifically, these cores targeted locations with seismic indications of hydrates, gas, and deep sediments of interest (Simonetti et al., 2013). JPC-3 (Figure 5, 6) acts as a background control site, due to its location, being up-dip from the mound and the least affected by mound activity, but still close to the mound. JPC-6 targeted a gas chimney along a synthetic fault. Sediments recovered were slightly disturbed and gassy. JPC-2 did not have free gas or gas hydrate and was collected to find the oldest stratigraphic constraint with a 20 m core. This study will focus on the upper 2 meters of these three cores, which record erosional and depositional processes of the most recent mound activity.

1.3.5 δ 18O ANALYSIS

Oxygen stable isotope stratigraphy is based on the relationship between ^{18}O and ^{16}O in a given sample. Foraminifera shells of calcium carbonate contain oxygen of different isotopic composition depending on water salinity, temperature of surrounding water, and the amount of water in ice sheets (Williams, 1984). Glacial-interglacial paleoclimatic cycles, associated eustatic change, and relative dating can be done using oxygen isotope analysis in the Gulf of Mexico. The ^{18}O /^{16}O of seawater becomes more positive during glacial times due to Rayleigh Distillation of oxygen isotopes where more light ^{16}O molecules are being stored in glacial ice (Williams, 1984). These ratios become more negative during interglacial periods when glacial water is returned to the oceans (Williams, 1984). Glacial sediments are represented by more positive δ 18O values and Holocene interglacial sediments have a stronger negative δ 18O isotope ratio (Williams, 1984). $\delta^{18}O$ sediment core analysis was done using Isoprime stable isotope ratio mass spectrometer. The upper 2 meters of JPC-2, JPC-3, and JPC-6 were sampled for 20 cc's

at a 5 cm interval. Foraminifera were cleaned of fine-grained sediments using water and a 63 micron sieve. The sediment was dried and picked for the species Globigerinoides Ruber due to its presence throughout the Last Glacial Maximum (LGM) and the most recent deglaciation. This species is then washed in methanol and sonicated. The foraminifera are transferred to vials and put into the mass spectrometer. The mass spectrometer ionizes the CO2 molecules into positively charged ions and separated into different ion beams. The ratio of the beam intensities yields the 18O /16O ratio. δ 18O values are reported relative to a universal powdered belemnite from the Cretaceous Pee Dee Formation of South Carolina. δ 18O data from the Hat-03 core published in Ingram et al. (2010, 2013) was given to us courtesy of Dr. Wes Ingram and Dr. Stephen Meyers and is included in the results section.

1.3.6 BIOSTRATIGRAPHY

The species Globigerinoides Menardii repopulated the Atlantic ~7,000 years ago (Broeker et al., 2014). This species was not present during the LGM or before until Marine Isotope Stage 5 (Martinez et al., 2007). The presence of this species in the shallow gravity cores is used as an indicator of deposition during the Holocene. This is used in conjunction with oxygen stable isotope stratigraphy.

1.3.7 RADIOCARBON DATING

5 mg of planktonic foraminifera were picked from the sediment for radiocarbon dating. Radiocarbon dating was done by Keck Carbon Cycle AMS Facility at UC Irvine as fractions of the Modern standard, D14C, using the conventions of Stuiver and Polach (1977). Backgrounds of sample preparation were subtracted based on measurements of 14C-free calcite.

1.3.8 SOURCES OF ERROR/UNCERTAINTY

The use of the constant time-depth conversion of 1500 m/s represents an inaccuracy in isochore maps and depth to horizons. Lack of velocity data for the sediment requires a time-depth conversion to be done based off a constant velocity which is a misrepresentation of the actual velocity of the sediment. This sediment velocity could be inaccurate which changes the depth to horizons and stratigraphic layers. By correlating the red band in the sediment with the horizon picked as the red band in the time-depth converted seismic data there is an inaccuracy of up to 30 cm between the depth to horizon and depth to red band. The average inaccuracy of this was +/- 11%. This could be a result using a constant time-depth conversion or sediment cores not located directly on the seismic line collected or inclination of cores.

The methods of collecting sediment cores could cause mixing within the cores and the cores may not be collected perpendicular to the seabed. An inclination of 30 degrees with a sample of interest at 2 meters depth could cause the sediment recovered to appear to be from the depth of 2.3 meters. This could cause a mismatch between the depth to the sediment of interests in the seismic and sediment sampled in the cores.

There is a degree of uncertainty in the radiocarbon data (Figure 8) and the process of using different planktonic species could cause inaccuracies in the sediment time of deposition. In sampling foraminifera for radiocarbon dating, there is bioturbation and we may have sampled on the unconformity and as a result have sediment from both above and below the unconformity used to radiocarbon date the gap in sediment, specifically sample 3 from JPC-02 (Figure 6, 8).

1.4 RESULTS

1.4.1 EVIDENCE OF MOUND INITATION AFTER LAST GLACIAL MAXIMUM

Prior to deposition of the red band, or meltwater pulse 1A (Figure 3, 4), there is quiescent sedimentation (Figure 4) and no evidence for recent methane derived authigenic carbonates. After the red band there is a change in depositional patterns at MC-118 with stratigraphic thinning onto the mound and the red band truncating the sea bed in an angular unconformity (Figure 3). Bathymetric relief and structural components of the mound (Figure 3, 4) appear to have developed after the deposition of the red band because there is predominately uniform sedimentation prior to the red band and the faults cut through the red band with uniform offset to the underlying stratigraphy (Figure 3). Authigenic carbonates are present at the seabed, but there is no evidence for recent authigenic carbonate deposition before the red band chronostratigraphic boundary. Predominately uniform deposition over the study area is observed in the CHIRP data throughout the LGM and prior to the LGM (Figure 4). After the LGM and deposition of the red band, structural and stratigraphic features of the cold seep system were created. Results based on integrating seismic data and published core data (Ingram et al., 2010, Ingram et al., 2013) suggests tectonic activity and consequentially Woolsey Mound's initiation occurred within the last ~12ky after deposition of the red band (Figure 3, 4).

1.4.2 EVIDENCE OF SEDIMENTARY DRAPE AND TECTONIC TERMINATION

There is a shallow sedimentary drape visible in the seismic data that overlays faults and eroded sediment on the mound and is in angular unconformity with the underlying stratigraphy (Figure 3). The drape is in unconformity over the mound and disconformity moving out of the uplifted mound area to a conformable surface further out

from the mound superstructure (Figure 3). The thickness of the drape varies from ~10 to ~30 cm over Woolsey Mound and most of the MC-118 lease block based off seismic, δ 18O, radiocarbon dates, and biostratigraphy (Figure 3, 4, 5, 6). δ 18O, radiocarbon dates, and biostratigraphy of the JPC's reveals glacial sediment unconformably overlain by Holocene sediment, confirming the presence of a sedimentary drape (Figure 6). JPC-3 and Hat-03 δ 18O, and radiocarbon values show a conformable section and record the sea-level transgression (Figure 6). The red band correlates in Hat-03 and JPC-03 with spikes of more negative δ 18O values (Figure 6). The unconformable cores JPC-2 and JPC-6 record sediments deposited during the LGM overlain by recent Holocene sedimentary drape material without the visible red band (Figure 6). JPC-06 radiocarbon dates suggest a gap of ~9.5kya over the unconformity (Figure 6). The JPC-02 radiocarbon dates do not effectively record the unconformity, likely due to bioturbation of sediment, however biostratigraphy and δ 18O values record the unconformity. The presence of the unconformity suggests that uplift and faulting is no longer occurring at Woolsey Mound.

1.5 DISCUSSION

1.5.1 INITIATION OF THE WOOLSEY MOUND COLD SEEP SYSTEM

Though there are currently no radiometrically derived chronological data of authigenic minerals at this site, chronostratigraphic and structural relationships provide a reliable interpretation for cold seep activation. Previous Gulf of Mexico studies have dated cold seeps by U/Th and radiocarbon dating of methane derived authigenic carbonates and have found the timing of carbonate precipitation at cold seeps to vary (Bian et al., 2013, Feng et al., 2010, Aharon et al., 1997). Woolsey Mound appears to have become active after

the LGM and into the most recent sea-level high stand. This signifies that the depressurization of gas hydrates as a result of a decreased hydrostatic pressure and a drop in sea level or changes in water temperatures during the LGM was not the trigger for Woolsey Mound initiation. Based off correlating structural features of the mound and the creation of hydrocarbon migration pathways through faults, salt-tectonism appears to have been the trigger for mound initiation. High sediment input into the study area (Ingram 2010) combined with a rise in sea level may have changed the stress field of the subsurface near Woolsey Mound and caused the salt to move due to its unique rheology. Salt may have been sourced from the submarine canyon observed in the NE corner of MC-118 where there is faulting that appears to have occurred at the same time as Woolsey Mound formation. Salt withdrawal from this area and subsequent Woolsey Mound uplift may have created the migration pathways for this cold seep and gas hydrate system to become active. Further constraints on mound initiation could be made by radiometrically dating the authigenic carbonates present at Woolsey Mound. This would provide the time at which methane flux and resulting authigenic carbonate precipitation began and an archive of fluid flow at the hydrate and cold seep site.

1.5.2 GULF OF MEXICO COLD SEEPS

Roberts and Carney (1997) propose a model by which increased cold-seep initiation is linked to salt tectonism, sea level, and sedimentation where salt movement is a function of sea-level and sediment input in the Gulf of Mexico. Therefore, hydrocarbon flux into the oceans and subsequently the atmosphere is affected by increased salt movement in the Gulf of Mexico and may be related to sea-level fluctuations. In this model, cold seep activation is a result of salt tectonism which creates the migration

pathways for thermogenically derived hydrocarbons to leak from reservoirs. Increased sediment loading during the sea-level lowstand followed by a rise in sea level may cause activation of salt tectonism due to changes in stress fields on underlying salt bodies in the Gulf of Mexico. U/Th dating of Gulf of Mexico authigenic carbonates have identified precipitation of authigenic carbonates at two deepwater cold seep sites between 12 and 13 ky. (Feng et al., 2010) which appear to have become active through this process. Aharon et al. (1997) and Roberts et al. (1990) identifies other seep sites initiated following the LGM at ~12 ky linked to similar processes. Chen et al. (2007) identified carbonate precipitation during the middle Holocene attributed to fracture induced fluid flow from thermogenic sources. Furthermore this increased in thermogenic hydrocarbon flux associated with increased salt movement and sea-level has been observed at non-hydrate bearing shallow (260 m b.s.f.) sites (Bian et al., 2013). This study provides structural evidence of salt driven tectonic activity initiated seep flow within the last ~12ky that may be linked to these processes. However, salt tectonics is a complicated process that may not be affected by a uniform increase in hydrostatic pressure.

1.5.3 TECTONIC TERMINATION OF WOOLSEY MOUND COLD SEEP SYSTEM AND CURRENT HYDROCARBON FLUX

Tectonic activity at Woolsey Mound appears to have occurred within a short geologic time of <8ky and has since ceased (Figure 7). The presence of a sedimentary drape that is not faulted is indicative of tectonic termination (Figure 3, 5, 6, 7). Based off deposition rates (Ingram et al., 2010) and radiocarbon dates we expect this drape to have been depositing over the mound and surrounding areas for ~4ky. Erosional processes are interpreted to be related to deep sea currents visible in channels (Figure 3). The

unconformable sediment overlaying eroded sediment is indicative that these currents no longer are significantly eroding the mound, suggesting that bathymetric relief is no longer being created by salt tectonism and salt movement has ceased (Figure 3, 4, 6, and 7). This is observable where there is visible offset on the fault leading up towards the seafloor, but no fault scarp at the seafloor or through the sedimentary drape (Figure 3). Since there is no active observable fault movement, current hydrocarbon flux through faults to the seafloor may be controlled by hydrate formation/dissociation along theses faults, reservoir sourcing, or other factors discussed by Macelloni et al. (2013) and Simonetti et al. (2013).

1.6 CONCLUSION

This study constrains tectonic activity at a cold seep site, documenting the onset and tectonic termination of mound activity. Tectonic activity, associated with the underlying salt body, appears to be the reason for the onset of Woolsey Mound cold seep system. This occurred after the LGM, within the last ~12ky and was therefore likely not caused by the depressurization of gas hydrates during a sea level lowstand. This study provides insight into the tectonic governance of thermogenic cold seep initiation. Documentation of overlying unconformable sediment suggests quiescent tectonism at Woolsey Mound. Short-term time variant hydrocarbon flux may be a result of hydrate formation/dissociation, but initiation of hydrocarbon flux to the seafloor may be attributed to salt driven seismic activity after the LGM.

FIGURES

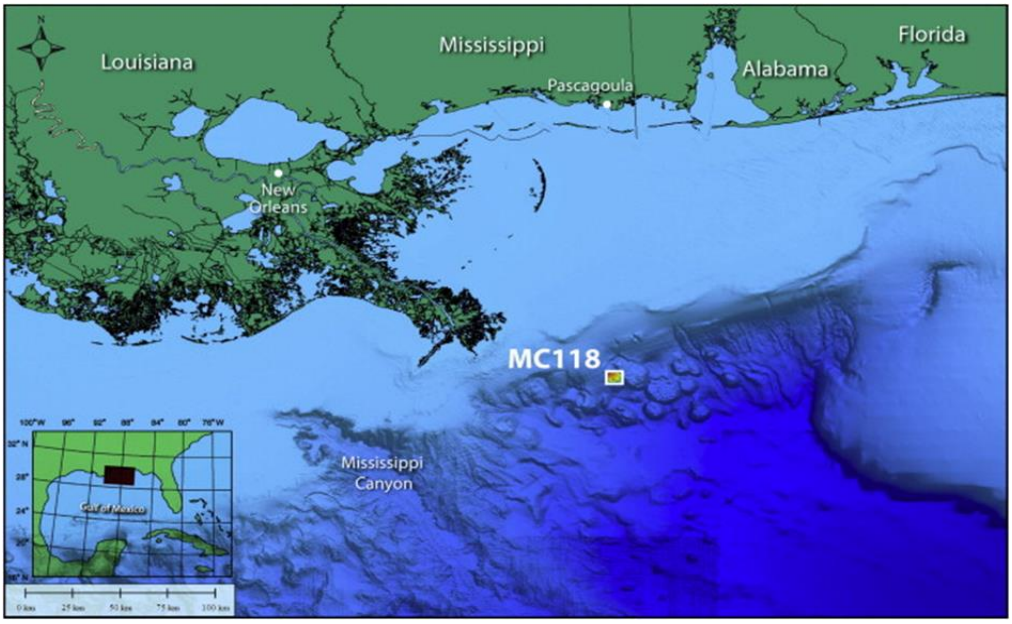

Figure 1.1. Location map of Woolsey Mound (lease block MC118) on middle slope, Northern Gulf of Mexico (Simonetti et al., 2013).

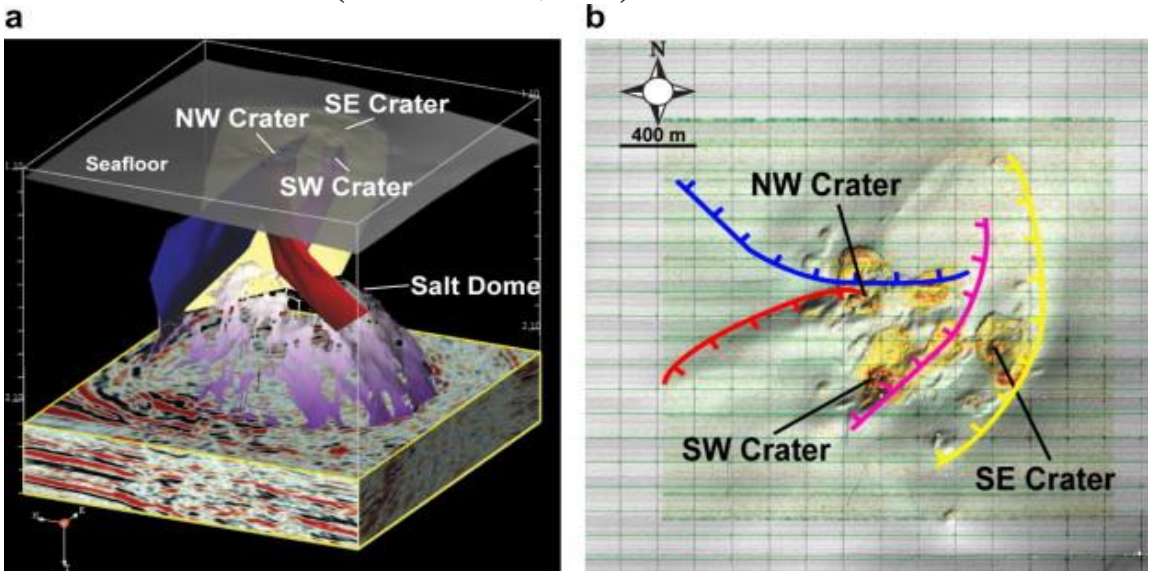

Figure 1.2. Salt dome ~300 m b.s.f. and master faults that act as migration pathways for hydrocarbons to the sea floor where they form craters, authigenic carbonates, gas hydrates and other stratigraphic features (Macelloni et al., 2012).

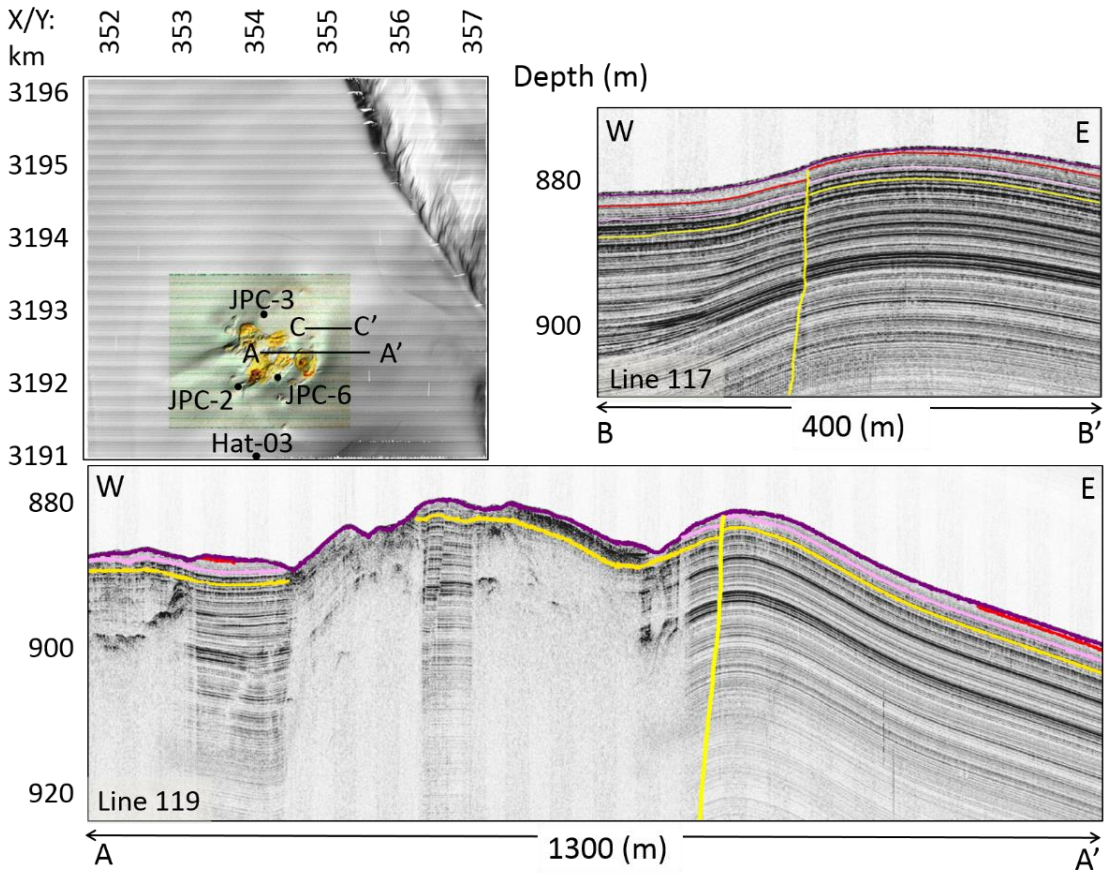

Figure 1.3. Cross section A-A' shows the presence of the red band ~14ka horizon within the mound superstructure (left) suggesting uplift post-dates deposition of the red band and overlying stratigraphy that is not part of the drape providing an age constraint to mound formation ~12ka based off deposition rates. Also, the red band truncating the drape in an angular unconformity suggesting mound formation is post-deposition of this stratigraphic unit. Cross section B-B' shows faulting goes through the red band and underlying stratigraphy with uniform offset, but not the drape or seafloor suggesting faulting precluded deposition of the drape and occurred after deposition of the red band.

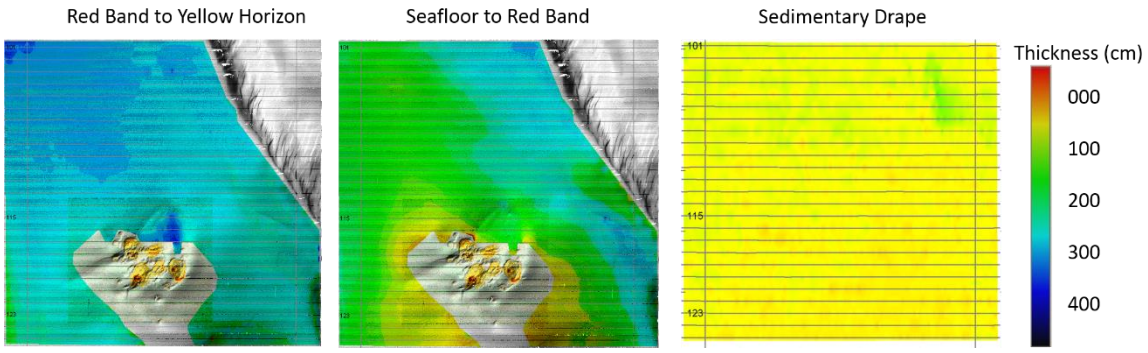

Figure 1.4. Isochore maps (true vertical thickness) for Late Pleistocene to Recent section at MC-118 (exclusive of NE corner of lease block). Quiescent sedimentation prior to deposition of "red band" (Left) ~19ka-14ka sedimentation showing a variance of only ~1m. ~14ka-present sedimentation showing a variance of ~4m and the truncation of the red band with the seabed (Middle). Presence of drape over the entire mound indicates erosional processes and tectonic uplift has ceased providing an age constraint of mound termination to ~4ka (Right).

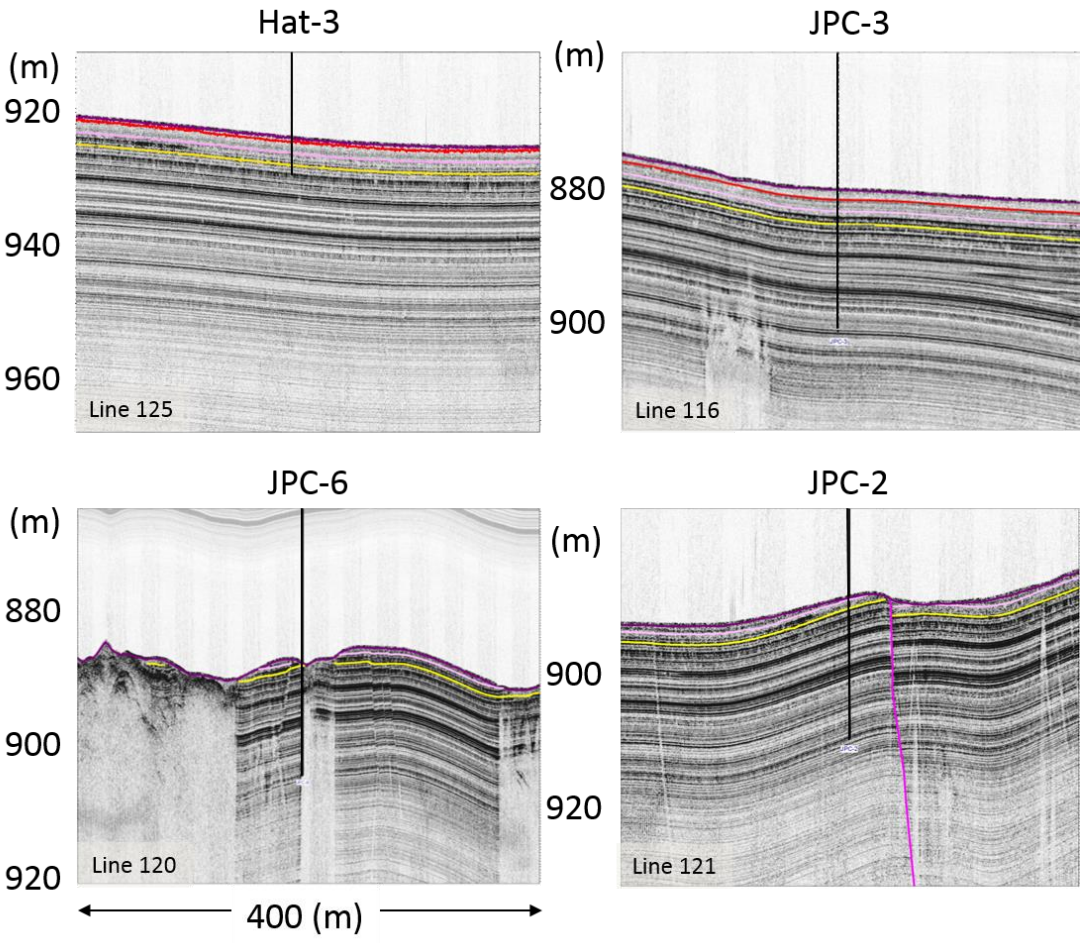

Figure 1.5. Projection on CHIRP profiles of four cores (Hat-3, JPC-2, JPC-3, and JPC-6) analyzed for oxygen isotope stratigraphy, radiocarbon dating, and biostratigraphy. Where preserved, red, yellow, and pink horizons are shown; base of drape shown in purple, section appears conformable at locations of Hat-3 and JPC-3, but clearly unconformable at locations of JPC-2 and JPC-6. Core locations relative to the mound structure can be seen in Figure 3.

δ 18 O

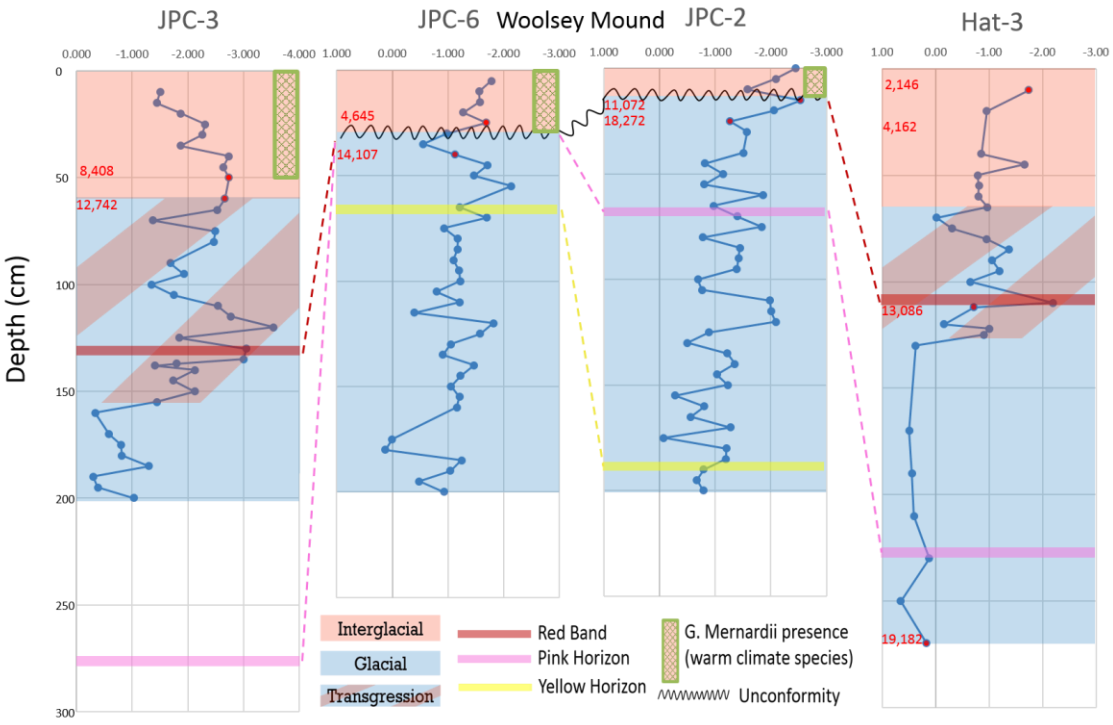

Figure 1.6. N-S core cross section over Woolsey Mound. δ 18 O data from G. Rubers showing the unconformable sediment on Woolsey Mound (JPC-2 and JPC-6), the deposition of the warm climate species G. Mernardii, and radiocarbon dates in calendar age written in red with associated locations highlighted in red dots. Hat-03 oxygen isotope stratigraphy and radiocarbon dates were provided by Dr. Wes Ingram and Dr. Stephen Meyers. Hat-03 radiocarbon date of 4,162 calendar age does not have an associated δ 18 O data point. G. Mernardii were picked to give biostratigraphic constraint of warm climate deposition (Broeker et al., 2014). The horizons locations are based off seismic data, and used to understand the extent of erosion. The red band is visible within the sediment and is recorded based off its location within the sediment cores. Seismic analysis suggests that JPC-6 has been eroded to a greater extent than JPC-2 (Figure 5), but radiocarbon dates below the unconformity in these cores suggests otherwise which may be related to sampling uncertainties discussed earlier.

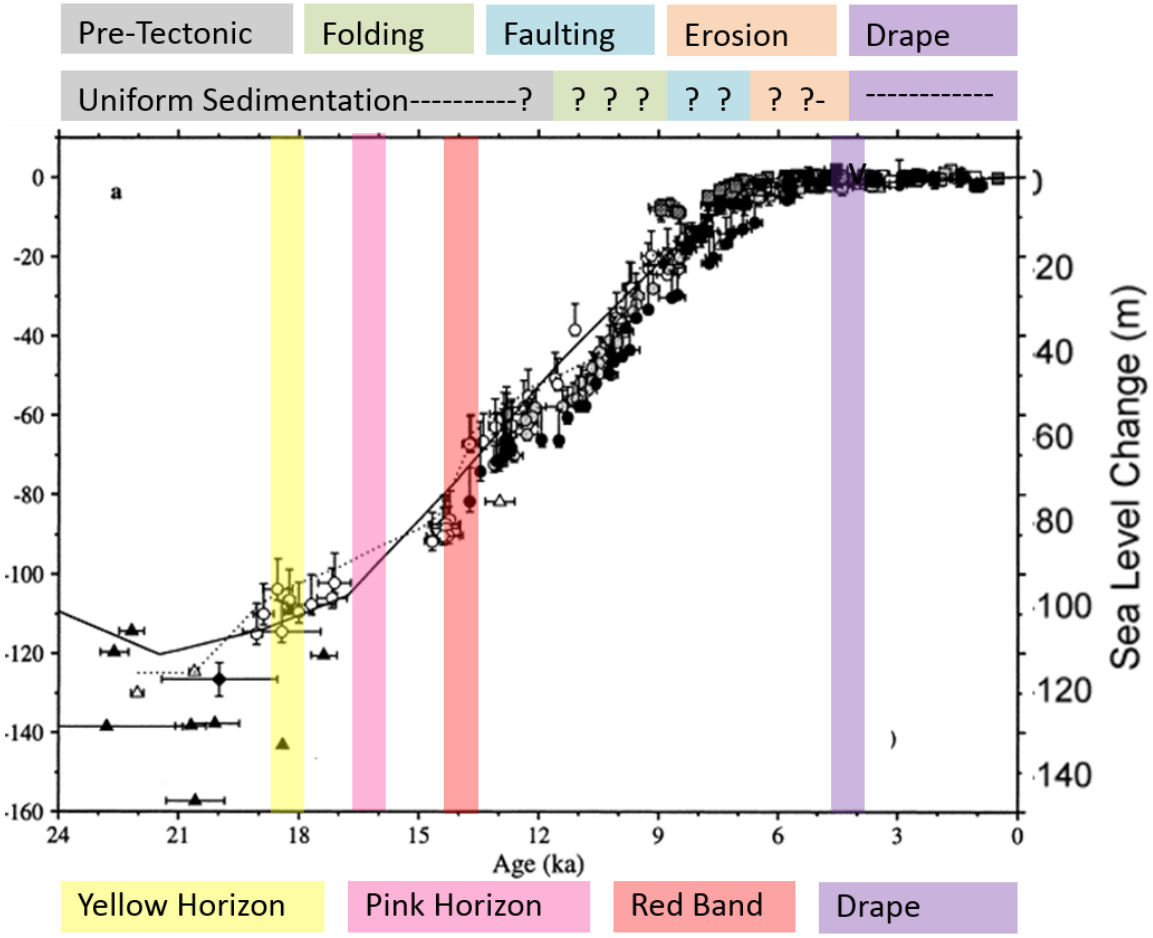

Figure 1.7. Sequence of geologic events at Woolsey Mound in relation to sea level (modified after Fleming et al, 1998). Modern mound activity began no earlier than ~12ka and concluded no later than ~4ka based on the presence of the sedimentary drape. Question marks represent an unknown age but known relative age, and dashed lines represent a known age. The time of deposition associated with different horizons is represented by color on the graph and the age of the pink and yellow horizons are based off radiocarbon dates and expected sedimentation from Ingram et al., (2010).

Sample #	1	2	3	4	5	6
Core	JPC-06	JPC-06	JPC-02	JPC-02	JPC-03	JPC-03
Depth (cm)	25	40	15	25	50	60
Sample weight for o18 and c13 ^{analysis}(mg)	5.5565	6.0125	5.521	5.6614	5.6832	5.1772
c13	1.645	1.518	1.151	1.462	1.172	1.03
o18	-1.693	-1.128	-2.542	-1.266	-2.744	-2.666
G. Mernardi Presence	x	o	x	o	x	o
Fraction Modern	0.574	0.2078	0.2859	0.1463	0.3714	0.2457
+/-	0.001	0.0008	0.0008	0.0007	0.001	0.0008
D14C	-426	-792.2	-714.1	-853.7	-628.6	-754.3
+/-	1	0.8	0.8	0.7	1	0.8
^{14C} age (BP)	4460	12620	1055	15440	7955	11275
+/-	15	35	25	45	25	30
Median Probability	-2695	-12157	-9122	-16322	-6458	-10792
Calendar Age	**4645**	**14107**	**11072**	**18272**	**8408**	**12742**

Figure 1.8. Table of data collected and used to identify and characterize the unconformity. Sampling intervals for the unconformity were done based off $\delta^{18}O$ results and biostratigraphy. A reservoir calibration was applied the BP 14C dates to convert into Calendar Age before present.

REFERENCES

Aharon, P., Schwarcz, H.P., Roberts, H.H., 1997. Radiometric dating of submarine hydrocarbon seeps in the Gulf of Mexico. Geological Society of America Bulletin 109, 568-579.

Bangs, N.L., Hornbach, M.J., Berndt, C. 2013. The Mechanics of Intermittent Methane Venting at South Hydrate Ridge Inferred from 4D Seismic Surveying Earth and Planetary Science Letters, 310, 105-112

Bangs, N.L., Hornbach, Matthew, J., Moore, G.F., Park, O.J., 2010. Massive methane release triggered by seafloor erosion offshore southwestern Japan. Geology, v. 38 no.11; p. 1019-1022.

Bayon, G., Henderson, G., Bohn, M., 2009a. U–Th stratigraphy of a cold seep carbonate crust. Chemical Geology 260, 47–56.

Bayon, G., Loncke, L., Dupré, S., Ducassou, E., Duperron, S., Etoubleau, J., Foucher, J.P., Fouquet, Y., Gontharet, S., Henderson, G.M., Huguen, C., Klaucke, I., Mascle, J., Migeon, S., Olu-Le Roy, K., Ondréas, H., Pierre, C., Sibuet, M., Stadnitskaia, A., Woodside, J., 2009b. Multi-disciplinary investigation of fluid seepage on an unstable margin: the case of the Central Nile deep sea fan. Marine Geology 261, 92–104.

Bian, Y., Feng, D., Roberts, H.H., Chen, D., 2013. Tracing the evolution of seep fluids from authigenic carbonates: Green Canyon, northern Gulf of Mexico. Marine and Petroleum Geology, 44, 71-81.

Biastoch, A., Treude, D., Rupke, L., Rievesell, U., Roth, C., Burwicz, E., B., Park, W., Latif, M., Boning, C., W., Madec, G., Wallmann, K., 2011. Geophysical Research Letters, 38, L08602.

Boles, J.R., Clark, J.F., 2001. Temporal variation in natural methane seep rate due to tides, Coal Oil Point area, California. Journal of Geophysical Research, 106, 27,077-27,086.

Boswell, R., Collett, T.S., Frye, M., Shedd, W., McConnell, D.R., Shelander, D., 2012. Subsurface gas hydrates in the northern Gulf of Mexico, Marine and Petroleum Geology,34 (1), 4–30.

Brooker, Wally, Leopoldo, Pena, 2014. Delayed Holocene Reappearance of G. menardii. Paleocenography, doi: 10.1002/2013PA002590.

Brunner, C.A., 2011. Assessment of Cores from MC-118-0709, GC01, 02 and 04, Department of Marine Science, The University of Mississippi (Unpublished)

Chen, Y., R. Matsumoto, C. K. Paull, W. Ussler, III, T. Lorenson, P. Hart, and W. Winters 2007. Methane-derived authigenic carbonates from the northern Gulf of Mexico-MD02 Cruise,

Journal of Geochemical Exploration, 95, 1 – 15, doi:10.1016/j.gexplo. 2007.05.011.

Dickens, G.R., O'neil, J.R., Rea, D.K., and Owen, R.M., 1995. Dissociation of oceanic methane hydrate as a cause of the carbon isotope excursion at the end of the Paleocene. Paleocenography 10:965-971.

Fairbanks, Richard, 1989. A 17,000-year glacio-eustatic sea level record: influence of a glacial melting rates on the Younger Dryas event and deep-ocean circulation. Nature, v. 342, 637-642.

Feng, D., Roberts, H.H., Cheng, H., Peckmann, J., Bohrmann, G., Lawrence Edwards, R., and Chen, D., 2010. U/Th dating of cold-seep carbonates: An initial comparison. Deep-Sea Research II 57: 2055-2060.

Fleming, K., Johnson, P., Zwartz, D., Yokoyama, Y., Lambeck, K., Chappell, J., 1998. Refining the eustatic sea-level curve since the Last Glacial Maximum using far- and intermediate-field sites. Earth and Planetary Science Letters, 163, 327-342.

Hornbach, M., Lavier L., and Ruppel, C., 2007. Triggering mechanism and tsunamogenic potential of the Cape Fear Slide complex, U.S. Atlantic coastal margin, Geochemistry Geophysics Geosystems 8, Q12008

Ingram, W.C., Meyers, S.R., Brunner, C.A., Martens, C.S., 2010. Late-Pleistocene-Holocene sedimentation surrounding an active seafloor gas-hydrate and cold-seep field on the Northern Gulf of Mexico Slope. Marine Geology, 278, 43-53.

Ingram, W.C., Meyers, S.R., Martens, C.S. 2013. Chemostratigraphy of deep-sea Quaternary sediments along the Northern Gulf of Mexico Slope: Quantifying the source and burial of sediments and organic carbon at Mississippi Canyon 118. Marine and Petroleum Geology, 46, 190-200.

Judd, A.G., Hovland, M., 2007. Seabed Fluid Flow Impact on Geology Biology, and the Marine Environment. Cambridge University Press, Cambridge, UK.

Kannberg, P.K., Trehu, A.M., Pierce, S.D. Paull, C.K., Caress, D.W. 2013. Temporal variation of methane flares in the ocean above Hydrate Ridge, Oregon. Earth and Planetary Science Letters, 368, 33-42.

Kiel, Steffen, 2009. Global hydrocarbon seep-carbonate precipitation correlates with deepwater temperatures and eustatic sea-level fluctuations since the Late Jurassic. Terra Nova 21, 279–284.

Kutterolf, V., Libetrau, V., Morz, T., Freundt, A., Hammerich, T., Garbe-Schonberg, D. 2008. Lifetime and cyclicity of fluid venting at forearch mound structures determined by tephrostratigraphy and radiometric dating of authigenic carbonates, Geology, v. 36, 707-710.

Liebetrau, V., Eisenhauer, A., Linke, P., 2010. Cold seep carbonates and associated cold-water corals at the Hikurangi Margin, New Zealand: New insights into fluid pathways, growth structures and geochronology. Marine Geology, 272, 307-318.

Lutken, C.B., Brunner, C.A., Lapham, L.L., Chanton, J.P., Rogers, R., Sassen, R., Dearman, J., Lynch, L., Kuykendall, J., Lowrie, A., 2006. Analyses of core samples from Mississippi Canyon 118, paper OTC 18208. In: Presented at the Offshore Technology Conference. American Association of Petroleum Geologist, Houston, TX.

Lutken, C.B., Macelloni, L., Sleeper, K., et al., 2011. New Discoveries At Woolsey Mound, MC118, Northern gulf of Mexico Proceedings of the 7th International Conference on Gas Hydrates (ICGH 2011), Edinburgh, Scotland, United Kingdom, July 17-21, 2011.

Macelloni, L., Brunner, C.B., Caruso, S., Lutken, C.B., D'Emidio, M., Lapham, L.L., 2013. Spatial distribution of seafloor bio-geological and geochemical processes as proxies of fluid flux regime and evolution of a carbonate/hydrates mound, northern Gulf of Mexico. Deep-Sea Research I, 74, 25-38.

Macelloni, L., Simonetti, A., Knapp, J.H., Knapp, C.C., Lutken, C.B., 2012. Multiple resolution seismic imaging of a shallow hydrocarbon plumbing system, Woolsey Mound, Northern Gulf of Mexico. Marine and Petroleum Geology (2012), 38, 128-142.

Martinez, J.L., Mora, G., Barrows, T.T., 2007., Paleocenographic conditions in the western Caribbean Sea for the last 560 kyr as inferred from planktonic foraminifera, Marine Micropaleontology., 64, 177-188.

Mazumdar, P.A, Dewangan, H.M., Joao, A., Peketi, V.R., Kholsa, M., Kocherla, F.K., Badesab, R.K., Josh, P., Roxanne, P.B., Ramamurty, S.M. Karisiddaiah, D.J., Patil, A.M., Dayal, T., Ramprasad, C.J., Hawkesworth, R. Avanzinelli, 2009. Evidence of paleo-cold seep activity from the Bay of Bengal, offshore India. Geochemisty, Geophysics, Geosystems, 10, Number 6.

Nouze', H., Henry, P., Noble, M., Martin, V., and Pascal, G., 2004. Large gas hydrate accumulations on the eastern Nankai Trough inferred from new high resolution 2-D seismic data. Geophysical Research Letters, 31,

Roberts, H.H., Carney, R.S., 1997. Evidence of episodic fluid, gas, and sediment venting on the northern Gulf of Mexico continental slope. Economic Geology 92, 863-879.

Roberts, H., Aharon, P., 1994. Hydrocarbon-derived carbonate buildups of the northern Gulf of Mexico continental slope: a review of submersible investigations. Geo-Marine Letters 14, 135–148.

Sassen, R., Roberts, H.H., Jung, W., Lutken, C.B., DeFreitas, D.A., Sweet, S.T., Guinasso Jr., N.L., 2006. The Mississippi Canyon 118 Gas Hydrate Site: a Complex Natural System. Paper OTC 18132 Presented at the Offshore Technology Conference, Houston, TX.

Shedd, W., Boswell, R., Frye, M., Godfriaux, P., Kramer, K., 2012. Occurrence and nature of "bottom simulating reflectors" in the northern Gulf of Mexico J. Marine and Petroleum Geology, 34, pp. 31–41

Simonetti, A., Knapp, J.H., Sleeper, K., Lutken, C. B., Macelloni, L., Knapp, C,C., 2013. Spatial Distribution of Gas Hydrates from High-Resolution Seismic and Core Data, Woolsey Mound, Northern Gulf of Mexico. Marine and Petroleum Geology, 44, 21-33.

Simonetti, Antonello, 2013. Spatial and Temporal Characterization of a Cold Seep-Hydrate System (Woolsey Mound, Deep-Water Gulf of Mexico). University of South Carolina Ph. D. Thesis.

Sleeper, K.A., Lowrie, A., Bosman, A., Macelloni, L., Swann, C.T., 2006. Bathymetric Mapping and High Resolution Seismic Profiling by AUV in MC 118 (Gulf of Mexico). Paper OTC 18133 Presented at Offshore Technology Conference, Houston, TX.

Solomon, E.A., Kastrier, M., MacDonald, I.R., and Leifer, I., 2009. Considerable Methane fluxes to the atmosphere from hydrocarbon seeps in the Gulf of Mexico. Nature Geoscience 2:561-565.

Stuiver, M., Polach, H.A., 1977. Reporting of 14C Data. Radiocarbon, 19, 355-363.

Taylor, M.H., Dillon, W.P., and Pecher, I.A., 2000. Trapping and migration of methane associated with the gas hydrate stability zone at the Blake Ridge Diapir: new insights from seismic data. Marine Geology 164: 79-89.

Teichert, B.M.A., Eisenhauer, A., Bohrmann, G., Haase-Schramm, A., Bock, B., and Linke, P., 2003. U/Th systematic and ages of authigenic carbonates from Hydrate Ridge, Cascadia Margin: Recorders of fluid flow variations. Geochimica et Cosmochimica Acta, 67, 3845-3857.

Tong, H., Feng, D., Cheng, H., Yang, S., Wang, H., Min, A., Edwards, L. R., Chen, Z., Chen, D., 2013. Authigenic carbonates from seeps on the northern continental slope of the South China Sea: New insights into fluid sources and geochronology. Marine and Petroleum Geology, 43, 260-271.

Watanabe, Y., Nakai, S., Hiruta, A., Matsumoto, R., Yoshida, K., 2008. U–Th dating of carbonate nodules from methane seeps off Joetsu, Eastern Margin of Japan Sea. Earth and Planetary Science Letters 272, 89–96.

Williams, Douglas 1984. Correlation of Pleistocene Marine Sediments of the Gulf of Mexico and Other Basins Using Oxygen Isotope Stratigraphy, in: Healy-Williams, N. (ed.), Principles of Pleistocene Stratigraphy Applied to the Gulf of Mexico, International Human Resources Development Corp., Boston, pp. 65-118.

Wirsig, C., Kowsmann, R.O., Miller, D.J., Godoy, J.M.O., Mangini, A., 2012. U/Th-dating and post-depositional alteration of a cold seep carbonate chimney from the Campos Basin offshore Brazil. Marine Geology, 329-331, 24-33.

APPENDIX A SUPPLEMENTARY DATA

TABLE A.1 $\delta^{18}O$ AND $\delta^{13}C$ ANALYSIS

depthjpc-02	c13	o18		depthhat-03	c13	o18		depthjpc-03	c13	o18		depthjpc-06	13C	18O
0	1.361	-2.443		10	1.06	-1.74						5	1.425	-1.779
5	1.306	-2.087		20	1.42	-0.96		10	1.639	-1.502		10	1.636	-1.562
10	1.353	-1.592		40	0.82	-0.86		15	1.730	-1.445		15	1.559	-1.573
15	1.151	-2.542		45	0.80	-1.67		20	1.627	-1.875		20	1.599	-1.277
20	1.485	-2.057		50	0.44	-0.79		25	1.391	-2.313		25	1.645	-1.693
25	1.462	-1.266		55	1.16	-0.81		30	1.067	-2.259		30	0.968	-0.976
30	1.678	-1.574		60	0.68	-0.80		35	1.285	-1.870		35	1.188	-0.559
40	1.377	-1.505		65	0.67	-0.97		40	0.934	-2.741		40	1.518	-1.128
45	1.528	-0.814		70	1.05	-0.02		45	0.900	-2.633		45	1.300	-1.713
50	1.355	-1.138		75	0.18	-0.31		50	1.172	-2.744		50	1.341	-1.472
55	1.425	-0.803		80	0.74	-0.95		60	1.030	-2.666		55	0.972	-2.142
60	1.352	-1.865		85	0.85	-1.37		65	0.904	-2.532		65	1.365	-1.208
65	1.257	-0.968		90	-0.19	-1.06		70	1.036	-1.377		70	1.219	-1.694
70	1.430	-1.397		95	0.88	-1.20		75	1.105	-2.495		75	1.737	-0.925
75	1.221	-1.836		100	0.25	-0.65		80	0.903	-2.466		80	1.564	-1.178
80	1.259	-0.775		110	1.13	-2.19		90	1.364	-1.688		85	1.563	-1.172
85	1.526	-1.447		112	0.61	-0.72		95	1.192	-1.931		90	1.571	-1.098
90	1.412	-1.418		120	0.52	-0.16		100	0.994	-1.344		95	1.498	-1.203
95	1.490	-1.391		122	0.47	-1.00		105	1.140	-1.749		100	1.670	-1.219
100	1.390	-0.691		125	0.92	-0.91		110	1.172	-2.539		105	1.604	-0.792
105	1.340	-0.761		130	0.42	0.37		115	0.945	-2.767		110	1.644	-1.215
110	1.321	-1.988		170	0.84	0.49		120	0.908	-3.541		115	1.491	-0.397
115	1.313	-2.003		190	0.72	0.44		125	0.931	-1.846		120	1.559	-1.820
120	1.150	-2.090		210	0.94	0.40		130	1.155	-3.049		125	1.370	-1.578
125	1.294	-0.881		230	0.79	0.12		135	0.817	-3.006		130	1.136	-1.052
130	1.423	-0.500		250	0.71	0.65		137	1.062	-1.798		135	1.249	-0.910
135	1.080	-1.216		270	0.86	0.17		138	0.741	-1.411		140	1.249	-1.472
140	1.503	-1.352						140	0.943	-2.131		145	0.888	-1.226
145	1.178	-1.029						145	1.048	-1.737		150	1.301	-1.054
150	1.461	-1.226						150	0.729	-2.124		155	0.967	-1.206
155	0.992	-0.282						155	0.946	-1.443		160	1.311	-1.160
160	1.348	-0.804						160	0.447	-0.336		175	0.972	0.005
165	1.122	-0.561						170	0.748	-0.582		180	0.906	0.127
170	1.326	-1.275						175	1.300	-0.797		185	1.403	-1.243
175	1.377	-0.074						180	0.889	-0.816		190	1.400	-1.046
180	1.344	-1.202						185	1.162	-1.304		195	0.677	-0.485
185	1.577	-1.195						190	1.120	-0.295		200	1.497	-0.930
190	1.403	-0.793						195	1.286	-0.384				
195	1.247	-0.671						200	1.384	-1.028				
200	1.794	-0.786												

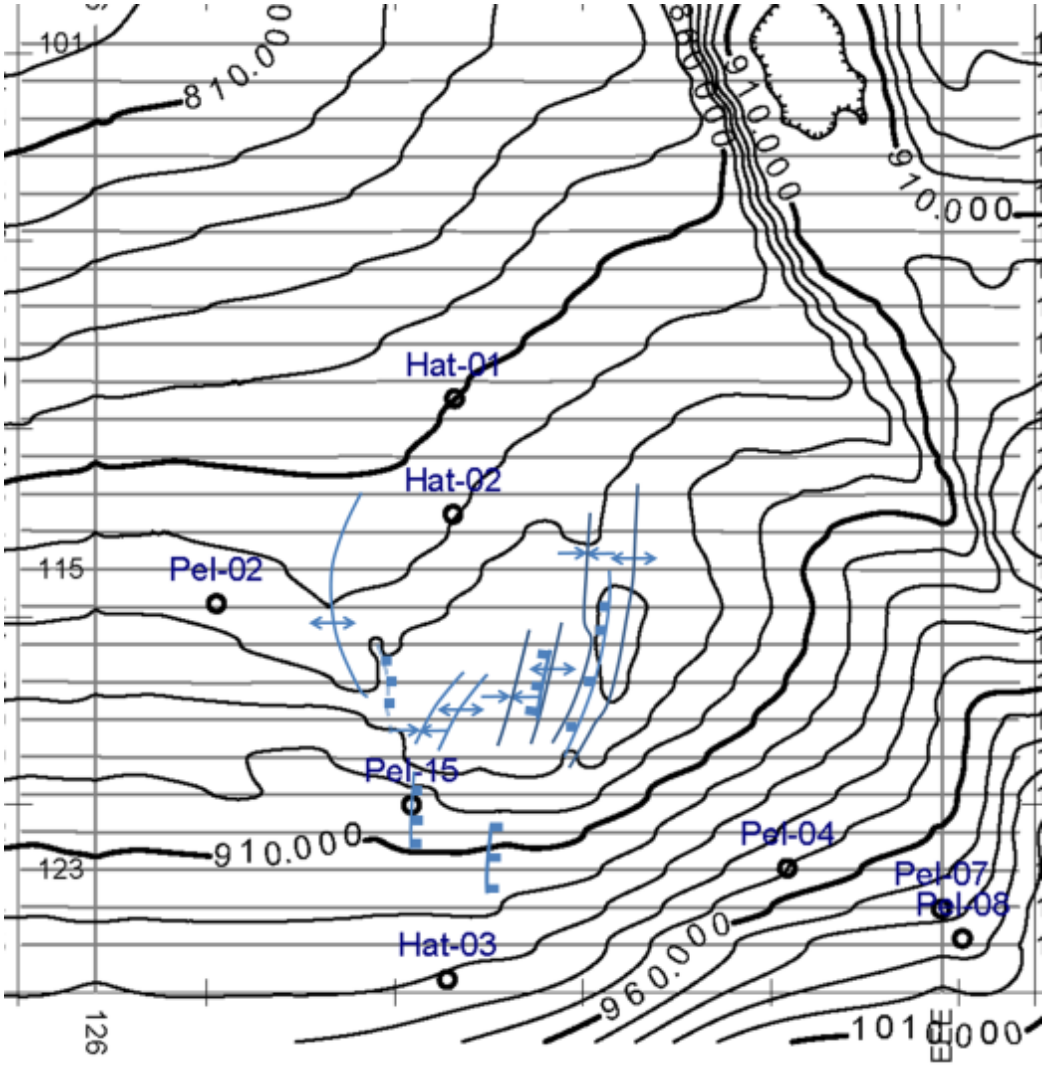

FIGURE A.1 STRUCTURAL AND BATHYMETRIC MAP OVER WOOLSEY MOUND